Journal of Science and Transport Technology
Journal homepage: https://jstt.vn/index.php/en

Analysing temperature distributions in turbine first-stage rotor blades of a helicopter turboshaft engine

Tien-Duong Le[1], Doan Cong Nguyen[2,*], Thanh Le Nguyen[3]
[1]Le Quy Don Technical University, 236 Hoang Quoc Viet, Hanoi, Vietnam letienduongdc23@lqdtu.edu.vn
[2]University of Transport and Technology, 54 Trieu Khuc, Thanh Xuan, Hanoi, Vietnam, doannc@utt.edu.vn
[3]Air Force Officer's College, No.03 - Villa Street, Tan Lap Ward, Nha Trang City, Khanh Hoa, Vietnam; thanhmbdc@gmail.com

Article info
Type of article:
Original research paper

DOI:
https://doi.org/10.58845/jstt.utt.2024.en.4.3.1-10

***Corresponding author:**
Email address:
doannc@utt.edu.vn

Received: 15/5/2024
Revised: 13/07/2024
Accepted: 18/7/2024

Abstract: In helicopter turboshaft engines, turbine blades operate under extreme conditions. With increasing engine power, the gas temperature following the combustion chamber can reach approximately 1300 K. The turbine rotors endure significant centrifugal forces due to their high rotational speeds. Additionally, they experience thermal and aerodynamic loads from the flow of combustible gases, which non-uniformly impact the turbine blades at high temperatures. Furthermore, the mechanical properties of turbine blade materials are limited and strongly influenced by operating temperatures. This article presents a numerical investigation focusing on the temperature distribution of first-stage turbine rotor blades that do not feature internal cooling channels. The results indicate the regions of peak temperatures and evaluate rotor blade strength. Comparative analysis between theoretical and numerical calculations of blade temperature distribution reveals minor disparities: approximately 30 degrees at the blade shroud, 8 degrees at the mid-span section, and 15 degrees at the hub. These variations amount to less than 3% at the shroud, 1% at the mid-span section, and 1.5% at the hub.
Keywords: high-pressure turbine, rotor blade, turboshaft, temperature.

1. Introduction

A helicopter powered by a turboshaft engine is capable of vertical takeoff and landing, as well as hovering and flying backwards. Turboshaft engines have significantly impacted the aviation industry, providing the necessary power with minimal weight penalty. Additionally, turboshafts can be scaled to fit the size of the helicopter, making it the preferred engine for almost all helicopter models in use today [1].

The turbine is a crucial component of turboshaft engines. It can rotate at speeds of up to 20,000 rpm (reaching 19,537 rpm) during takeoff [2], facing significant centrifugal forces. Additionally, the turbine is exposed to the extreme gas temperature after the combustion chamber, which can reach up to 1300 K [3-7].

Turbine blades frequently experience various types of damage during engine operation, such as thermal fatigue resulting in cracking (0), local overheating, corrosion-erosion damage (0), and burn-out areas (0).

0 [8] shows a crack on the nozzle blade of a high-pressure turbine. The crack appears to be

concentrated in the blade shroud, an area without cooling holes. These cracks are due to the excessive gas temperature impacting the blade, causing the local high temperature at these points, ultimately damaging the microstructure of the material used in the nozzle blade.

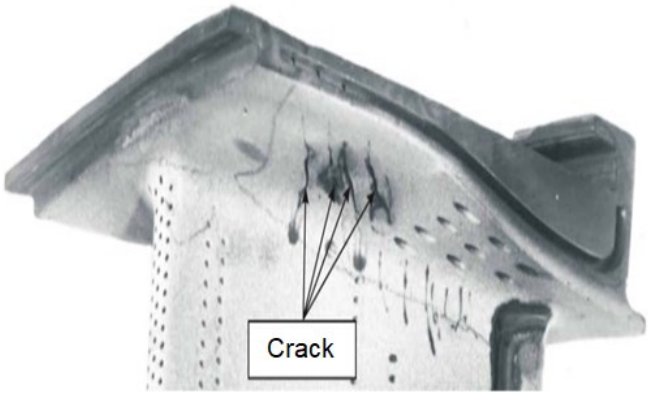

Fig 1. Crack regions on the nozzle turbine blade [8]

The combination of temperature, stress and oxidizing environment leads to diffusion processes in the surface layers of blades, thereby limiting their durability [9]. When a fuel-air mixture burns, it generates a gas flow characterized by high pressure, temperature and speed. In addition, turbine blades experience significant stress from centrifugal and gas-dynamic forces, as well as exposure to the harsh environment of combustion products and atmospheric air. Protective properties may decrease due to erosive wear caused by the high-temperature gas during operation.

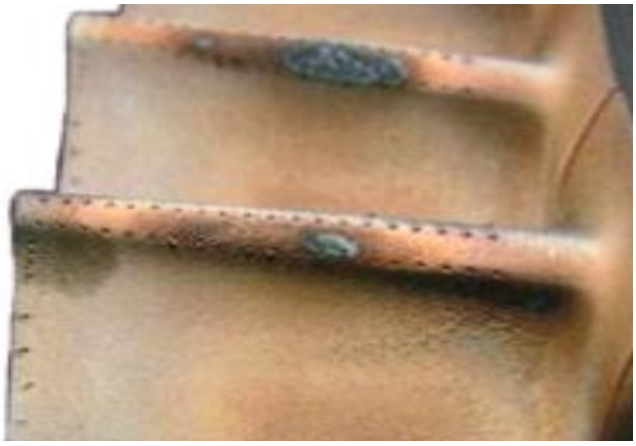

Fig 2. Corrosion-erosion damage on the leading edge of a high-pressure turbine blade [10]

Visible in 0 [10] is erosion-corrosion damage of the blade leading edge, resulting from numerous impacts of solid particles, leading to mechanical destruction of the coating. the high carbon content in fuel increases the erosive effect of the gas flow, accelerating coking on parts and sulfide corrosion, thereby amplifying the overall destructive impact.

0 [11] shows a photograph of burn-out blades of a first-stage high-pressure turbine due to overheating.

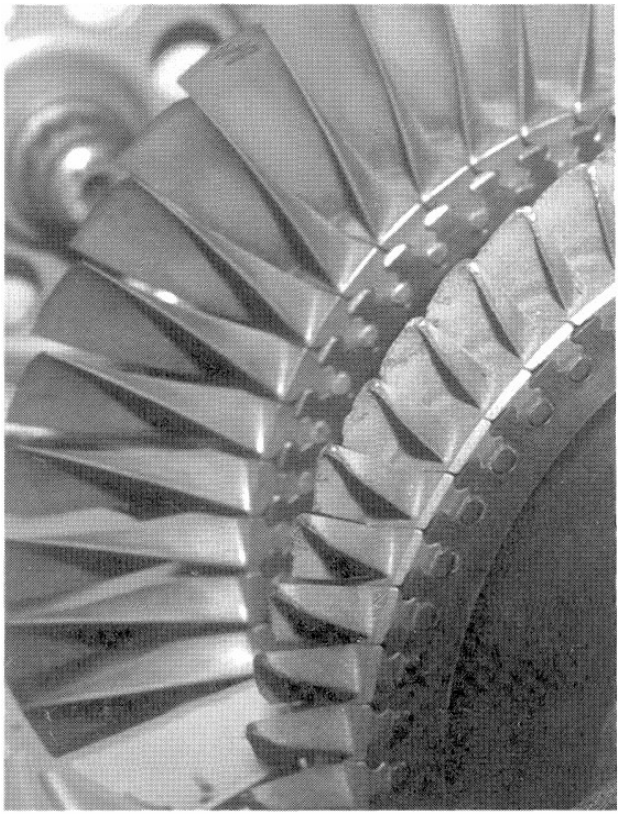

Fig 3. Burn-out turbine blades due to overheating [11]

Unfortunately, our country lacks the capability to manufacture gas turbine engines or replacement parts, particularly turbine components. Consequently, when damage occurs to turbine blades, the entire turbine components may be replaced, a process that incurs significant expenses [2]. Calculating the blade temperature distribution is the foundation for determining turbine blade durability and improving the blade temperature field.

The research conducted by Porreca L. et. al [12] aimed to enhance the efficiency of designing gas turbines. Their study focused on developing advanced calculation methods and tools for

determine the temperature distribution of turbine blades.

Meanwhile, Li Xu et. al [13] addressed the challenge of designing high-pressure turbine blades. Their study revealed that existing methods for calculating external heat transfer conditions lacked accuracy. As a result, their research aimed to devise a new, more precise method for calculating the external heat transfer of gas turbine blades. Through numerical and theoretical analysis, the blade temperature distribution was determined. These results are critical for understanding the stress distribution and evaluating the turbine blade durability.

During engine operation, the continuous combustion generates a high temperature and pressure flow, directly impacting the turbine blades. As a result, the blades experience to mechanical stress due to aerodynamic and centrifugal forces and undergo abrasion due to chemical corrosion. In addition, to identify the cause of blade damage, it is necessary to determine the thermal state, particularly in cases where the blades lack internal cooling channels.

Accurately calculating the temperature distribution is critical for assessing the reduction in strength of the blade material properties.

2. Numerical models

Various software packages are available for calculating fluid dynamics and blade temperature distribution, including Star CCM+, Numeca, Ansys CFX, and Fluent. However, for this work, the ANSYS CFX module [14] was chosen due to its advanced algorithms, which enable reliable, fast, and accurate solutions [15-19]. This solver is well-parallelized and offers a wide range of physical models capable of describing almost all phenomena related to fluid flow.

In this study, the Ansys CFX (Ansys 2023 R1) module is used to simulate the fluid dynamics within the flowpath of the first-stage turbine rotor of a TV3-117 turboshaft engine. It is important to note that these rotor blades lack internal cooling channels, thus the gas temperature will significantly affect to their working conditions. Subsequently, the temperature distribution is calculated and employed as input conditions for determining the stress field using the Steady-State Thermal Analysis module. This 1-way Fluid-Structure Interaction (Fig 4) approach allows for a comprehensive analysis of the thermal and mechanical behaviors of turbine blades (Fig 5).

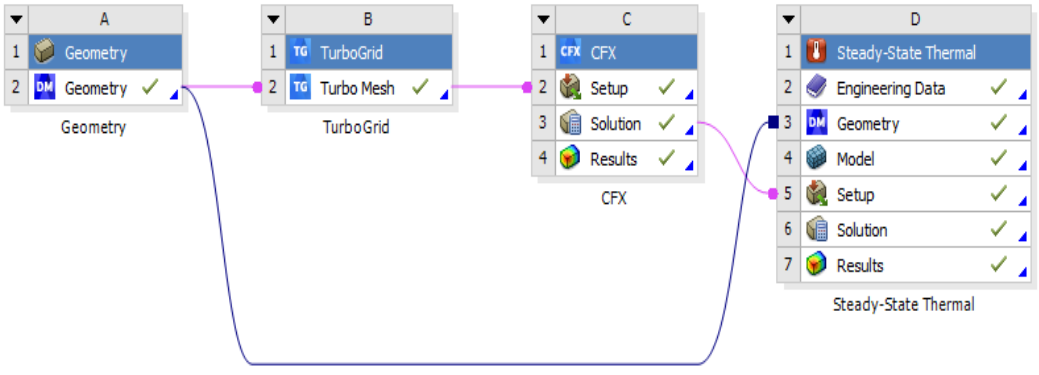

Fig 4. Computational model for calculating the blade temperature distribution

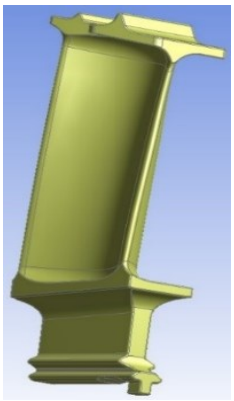

Fig 5. The turbine rotor blade of the TV3-117 turboshaft engine in NX 12

When conducting CFD calculations for the turbomachinery flowpath, it is advisable to use hexahedral elements. In this study, the meshing model was generated by TurboGrid module. However, to capture detail physical properties near the boundary layers betwwen the blade and gas flow, a mesh refinement has been implemented (Fig 6).

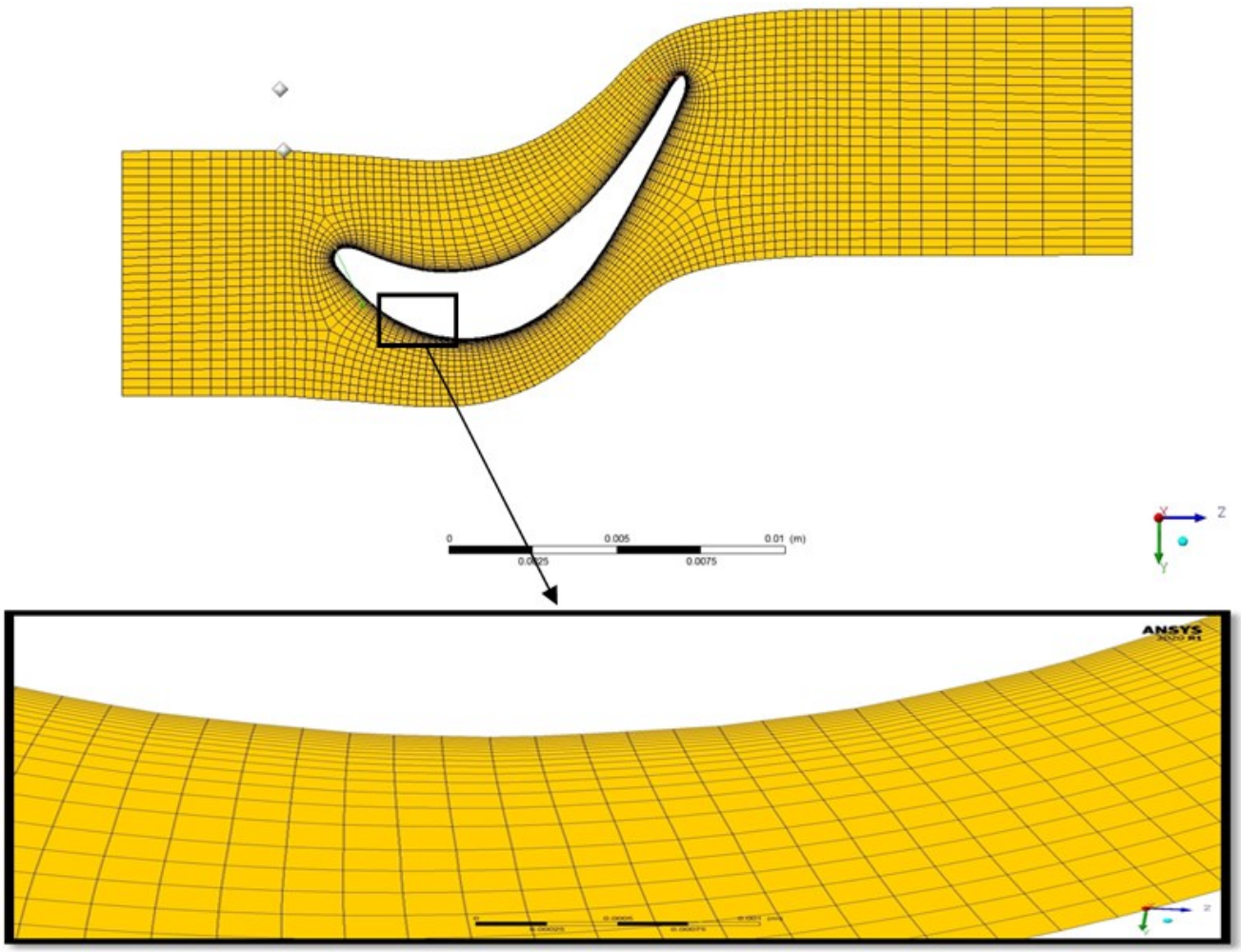

Fig 6. Blade cross-sectional mesh generated by TurboGrid module

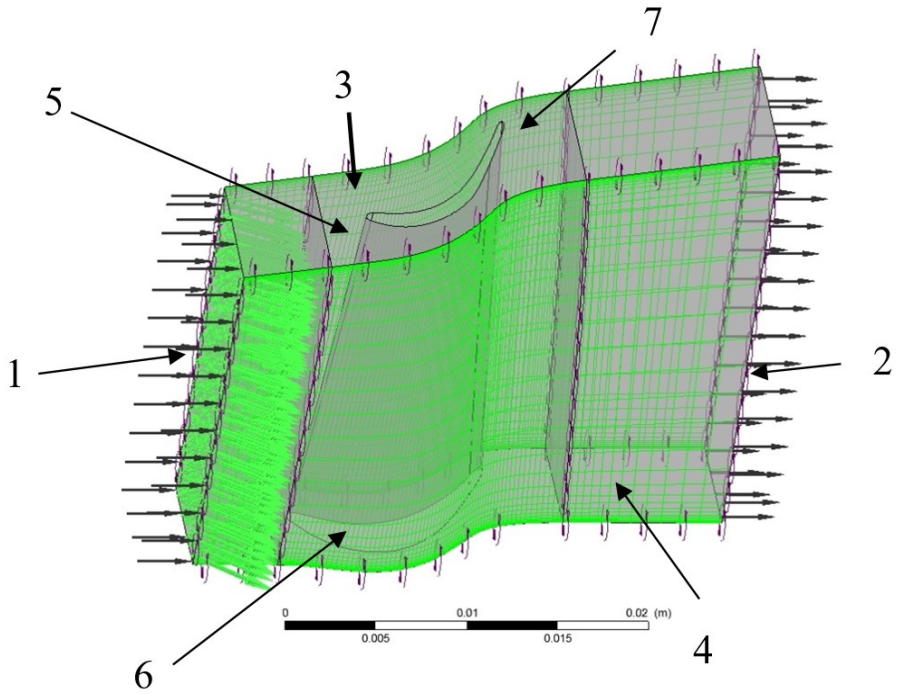

Fig 7. Boundary conditions at:
1. Inlet; 2. Outlet; 3. Shroud; 4. Hub; 5. Profile; 6,7. Periodic surfaces

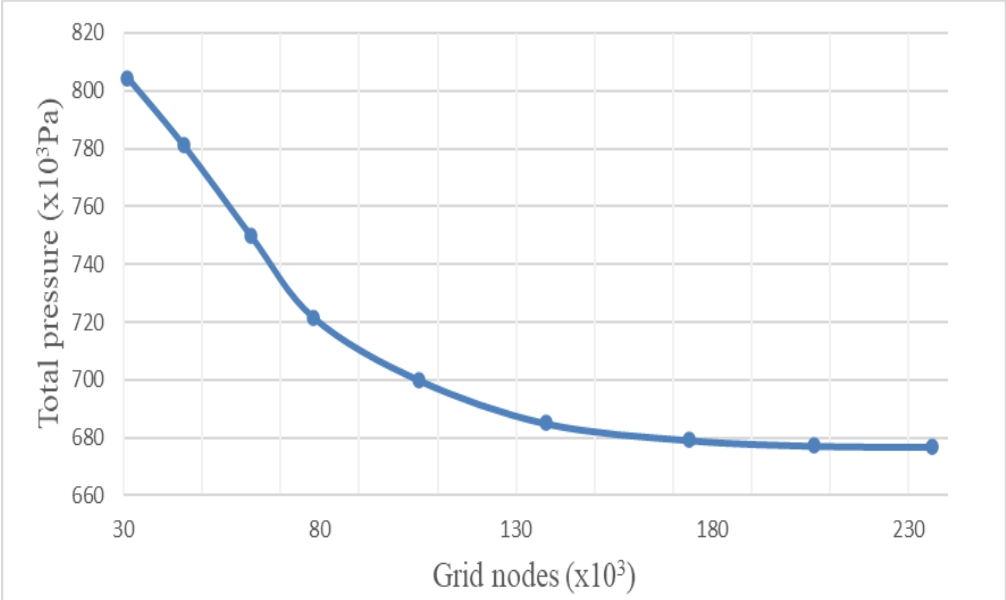

Fig 8. The total pressure at the outlet depends on the number of grid nodes

Set up the boundary conditions corresponding to take-off parameters in Fig 7, which represent the most critical engine operating mode, based on technical materials [20]. The following boundary conditions are applied: a total inlet pressure of 887120 Pa, a total inlet temperature of 1188 K, a turbine rotation speed of 19537 rpm, and an outlet static pressure of 591413 Pa [2],[6]. The working medium is the ideal gas under conditions of the energy conservation flow model (total energy), and the k-ω SST turbulence model. The convergence condition is set to $1e^{-4}$ or the least mean square RMS of 1%, with a maximum number of calculation steps set to 500 [9]. To ensure quality calculation results, the authors conducted research on the grid dependency of the number of grid nodes on the calculation results. The results are shown in Fig 8.

Thus, we see that when the number of grid nodes reaches over 105,000 to nearly 235,000, the total pressure behind the turbine blade changes very little. To facilitate calculations, the authors chose the number of grid nodes for the calculation to be 174086 nodes and 159720 elements. This mesh resolution is deemed acceptable and suitable for subsequent analysis steps.

To analyse the steady-state thermal conditions and use the results for calculating the blade temperature distribution in the Steady-State Thermal Analysis module. This analysis involves evaluating the thermal equilibrium of a system, where the temperature remains constant over time. In other words, it assesses the equilibrium system state subjected to constant thermal loads and environmental conditions [14],[20]. In this module, perform meshing with 149532 nodes and 85081 elements, as shown in 0. From the CFX calculation results, the "Convection Coefficient" is obtained as the constraint condition for the Steady-State Thermal Analysis, depicted in Fig 10.

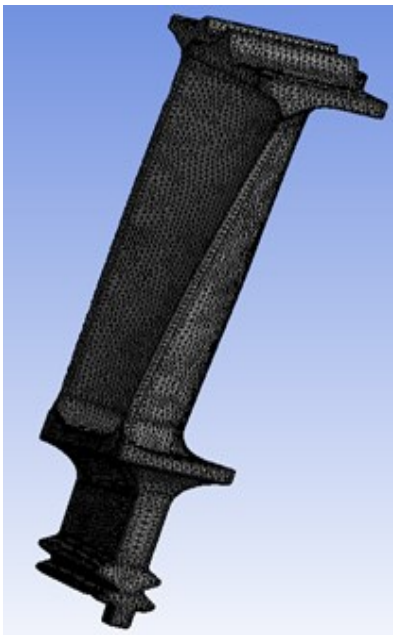

Fig 9. Meshing model of the turbine rotor blade

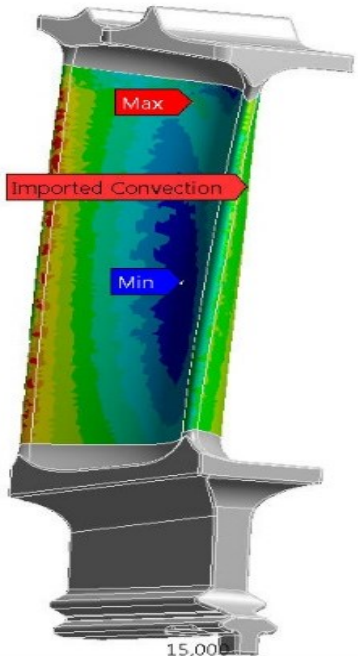

Fig 10. The boundary conditions in the Steady-State Thermal Analysis module, represented by imported convection coefficient

Table 1. The chemical composition in per cent of the heat-resistant alloy XH77TЮP [21]

Fe	C	Si	Mn	S	P
<1	<0.07	<0.6	<0.4	<0.007	<0.015
Cr	**Ce**	**Ti**	**Al**	**B**	**Pb**
19 - 22	<0.02	2.4 - 2.8	0.6 - 1	<0.01	<0.001

Table 2. Physical properties of XH77TЮP alloy [21]

T	$\alpha.10^{-6}$	λ	ρ
°C	1/°C	W/(m·°C)	kg/m^3
20		12.6	8200
100	12.67	13.9	8180
200	12.9	15.6	8140
300	13.3	17.2	8110
400	13.8	18.8	8070
500	14.2	20.9	8040
600	14.6	23.5	8000
700	15.1	25.1	7960
800	15.5	28.2	7920
900	16.2	31.1	7870

In there, T – temperature, °C; α - thermal expansion coefficient, 1/°C; λ - coefficient of thermal conductivity W/(m·°C); ρ - material density, kg/m^3.

The alloy manufactured for the turbine blades of the TV3-117 turboshaft engine is a heat-resistant and corrosion-resistant material, with properties equivalent to XH77TЮP (NiCr20TiAl) steel. The chemical composition of the material, excluding Nickel, is detailed in Table 1, where Nickel constitutes 70.07-77.4% of the alloy. The physical properties of the alloy, as detailed in Table 2, are inputted into the Engineering Data Module of Steady-State Thermal Analysis. These input parameters are essential for ensuring the accuracy and reliability of the numerical results.

3. Numerical results

The flow velocity gradually increases from the inlet section to the outlet, as depicted in 0. This is because some of the internal energy, specifically enthalpy, is converted into kinetic energy. This phenomenon occurs due to the conversion of internal energy, particularly enthalpy, into kinetic energy. The observed variation in gas flow velocity aligns with turbomachinery theory [21], validating the accuracy of the results and their applicability to subsequent calculations.

The gas temperature impacting the turbine blade varies along the contact surface, as illustrated in Fig 12. The high-temperature regions on the blade cross-section gradually decrease from the leading edge to the trailing edge. The highest temperatures are observed at the leading edge and shroud area, gradually decreasing at the trailing edge.

Fig 12, Fig 13 and Fig 14 demonstrates how the leading edge is exposed to a significant amount of heat directly from the hot gas, reaching temperatures of approximately 1077 K. Therefore, during operation, it is crucial to pay close attention to the gas temperature upstream of the turbine to prevent turbine blade damage due to overheating. These findings are consistent with the calculation process outlined in the documents [21-25]. In Fig 15, the temperature distribution is non-uniform,

with the highest temperature of 1048.5 K observed at the blade tip, while the leading edge represents a localized high-temperature region.

Fig 16 presents a comparison of numerical and theoretical results. According to the theoretical finding, the temperature along the turbine blade increases steadily from the hub to the tip. However, the numerical result show that the blade temperature distribution increases more slowly from the hub to the tip. This is due to the non-uniform distribution of the flow temperature. Specially, at the hub, the numerical results indicate a higher temperature compared to the theoretical outcome, whereas at the tip, the numerical result shows a lower temperature than the theoretical calculation. Nonetheless, the difference between these results is relatively minor. For instance, the temperature differences at the hub, mid-span and tip are approximately 15, 8 and 30 degrees, respectively. Such numerical results are acceptable for subsequent calculations determining the stress field and blade strength.

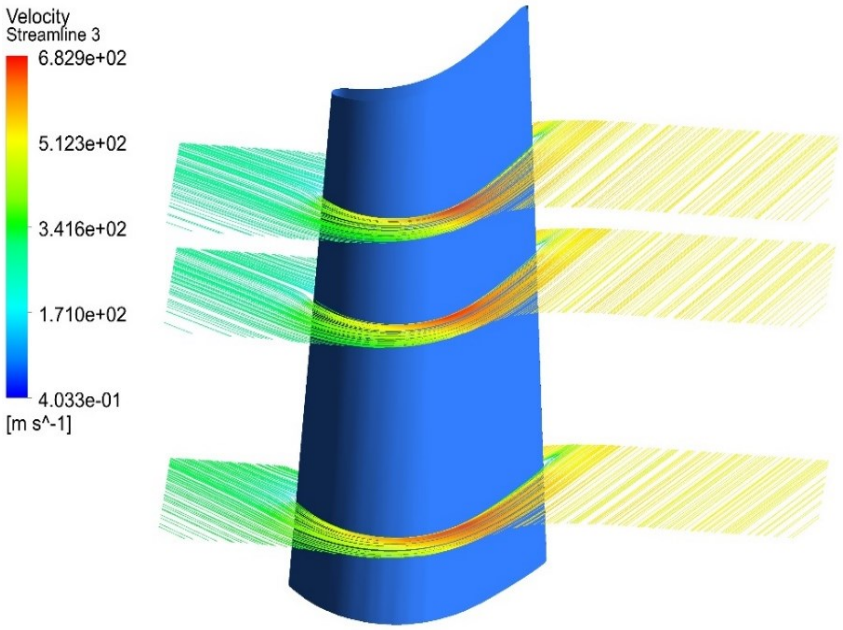

Fig 11. Flow velocity variation across blade spans

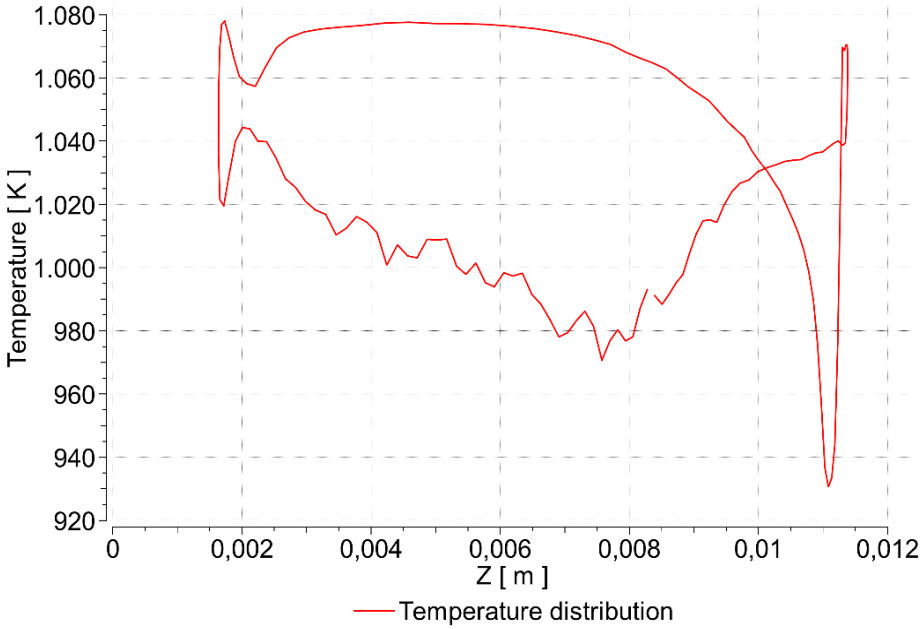

Fig 12. Temperature distribution on the averaged blade cross-section

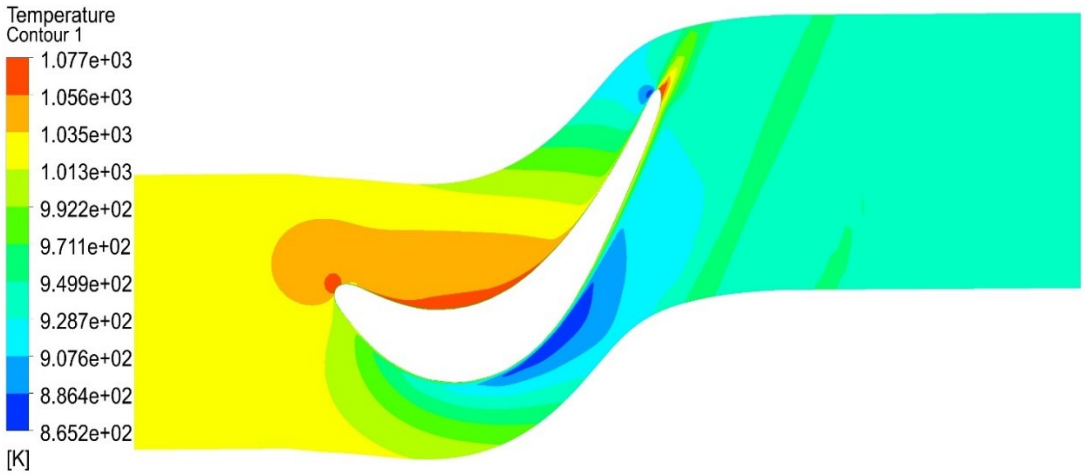

Fig 13. Temperature distribution on the averaged gas cross-section

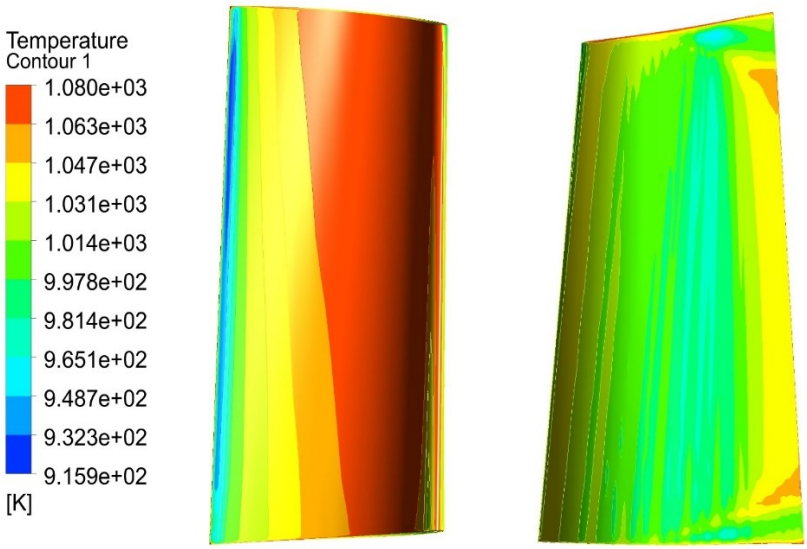

Fig 14. Temperature distribution contour of the gas flow around the turbine blade

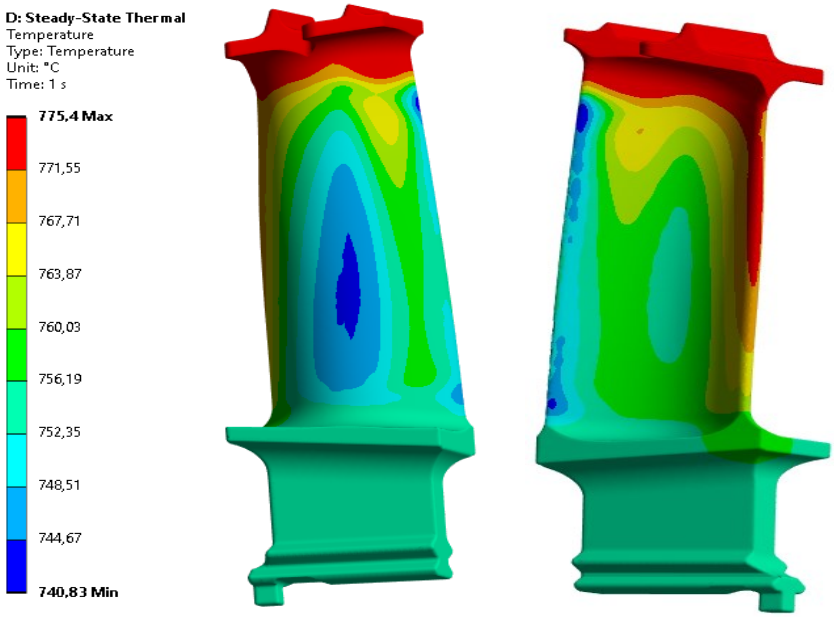

Fig 15. The temperature distribution on the turbine blade

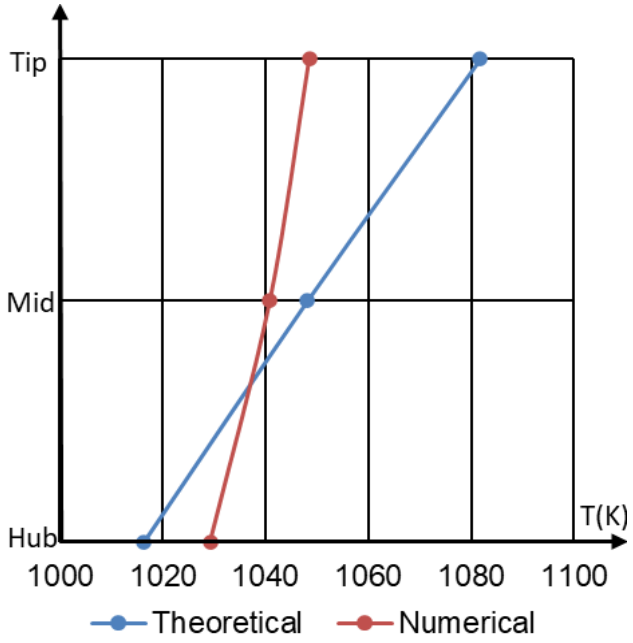

Fig 16. A comparison of the theoretical [10-12] and numerical results

4. Conclusions

This research has confirmed that the combustion gas upstream significantly affects the rotor blades of the first-stage turbine, particularly those lacking internal cooling channels.

The study employed numerical results obtained via the Ansys package, demonstrating consistency with theoretical calculations and falling within acceptable ranges. Analysis indicated that the leading edge of the blade experiences the highest temperatures. Moreover, due to the high rotational speeds during operation, the blades are subject to considerable stress. Consequently, the temperature plays a crucial role in determining the safety margin of the blades and, subsequently, impacts the engine's technical condition.

As a result, selecting appropriate blade materials during the engine design phase becomes crucial for ensuring stable operation and optimal performance, while simultaneously reducing the risk of catastrophic damage to the entire engine. This research is a foundation for assessing the safety factor of turbine blades at various cross-sections and understanding the blade temperature distribution. Aimed with this knowledge, improvements can be made to enhance the engine lifespan, thereby boosting its overall durability and reliability.

However, the current analysis overlooks the gas flow through the radial gap between the blade shroud and the turbine case. This aspect constitutes the next focus of the paper, aiming to assess the impact of gas flow through this gap on the blade temperature distribution.

References

[1]. W. Johnson. (1980). Helicopter Theory. *Dover Publications Inc. USA*.

[2]. A.D. Bogdanov, N.P. Kalinin, A.I. Krivo. (2000). Engine TV3-117. *Air Transport. Russian*.

[3]. Klimov. (1975). TV3-117 MT Free Turbine Turboshaft. In Engine Description and Maintenance Manual; Book 1/2. *Military Technical Academy: Bucharest, Romania*.

[4]. R.M. Catana, G. Dediu, C.M. Tarabic. (2022). Studies and Experimental Research in the Evaluation of TV2-117A Turboshaft Engine Working Regimes. *Applied Sciences*, 12(7), 3703.

[5]. J. Kurzke. (2005). How to Create a Performance Model of a Gas Turbine From a Limited Amount of Information. *Proceedings of the ASME Turbo Expo 2005: Power for Land, Sea, and Air, Reno, NV, USA; ASME GT 2005-68537; ASME: New York, NY, USA*, pp 145-153.

[6]. J.W. Chapman, T.M. Lavelle, J.S. Litt. (2016). Practical Techniques for Modeling Gas Turbine Engine Performance; NASA/TM-2016-219147. *Glenn Research Center: Cleveland, OH, USA*.

[7]. Klimov. (1986). TV3-117 Aircraft Technical Manual. *Klimov Ins. RU*.

[8]. A.A. Inozemsev, V.L. Sandratski. (2006). Gas turbine engines. *UEC Aviadvigatel. Russian*.

[9]. V.A. Leontiev, S.D. Zilichikhis, E.V. Kondratyuk, V.E. Zamkova. (2006). Restoring the performance of gas turbine engines using new technologies and materials. *Engine Building Bulletin*, 4, 99-103.

[10]. M.A. Petrova, M. Saadatibai, A.I. Tarasov.

(2015). Analysis of modern turbine engines working surface layers blades work conditions. *Civil Aviation High Technologies*, pp 124-127.

[11]. B. Meher-Homji, G. Gabriles. (1995). Gas turbine blade failures - causes avoidance and troubleshooting. *Proceedings of the 27th Turbomachinery symposium*, pp 129-180.

[12]. L. Porreca, T. Behr, J. Schlienger, A.I. Kalfas, R.S. Abhari, J. Ehrhard, E. Janke. (2005). Fluid Dynamics and Performance of Partially and Fully Shrouded Axial Turbines. *Journal of Turbomachinery*, 127(4), 668-678.

[13]. L. Xu, S. Bo, Y. Hongde, W. Lei. (2015). Evolution of Rolls-Royce air-cooled turbine blades and feature analysis. *Procedia Engineering*, 99, 1482-1491.

[14]. Ansys. (2023). Ansys CFX User's Guide. *Ansys Inc. USA*.

[15]. L. Lin, L. Cunliang, L. Wei, C. Wenbin, Z. Huiren, and X. Weijiang. (2023). Numerical research on the particle transport and deposition in the impingement-film cooling passage. *Physics of Fluids*, 35(5), 053302.

[16]. L. Luo, H. Yan, W. Du, L. Hou, Y. Fu, and S. Wang. (2023). Numerical analysis for film cooling characteristics of trenched hole under the effects of rib-disturbed feed flow and curved surface. *Physics of Fluids*, 35(3), 036105.

[17]. C. Wu, X. Yang, X. Tang, J. Ding, and P. Weng. (2023). Numerical investigation on flow and heat transfer mechanism of corrugated cooling channel in turbine blades. *Physics of Fluids*, 35(2), 026105.

[18]. A. Kumar and M. Pathak. (2023). Conjugate heat transfer analysis of internally cooled superalloy turbine blades with grooved channels. *Physics of Fluids*, 35(9), 095112.

[19]. H.M. Phan, P.H. Duan, and C.T. Dinh. (2020). Numerical aero-thermal study of high-pressure turbine nozzle guide vane: Effects of inflow conditions. *Physics of Fluids*, 32(3), 034111.

[20]. Ansys. (2023). Ansys Mechanical User's Guide. *Ansys Inc. USA*.

[21]. P.P. Walsh and P. Fletcher. (1998). Gas Turbine Performance. *Gas Turbine Performance. USA*.

[22]. Jack D. Mattingly. (1985). Elements of Propulsion: Gas Turbines and Rockets. *Cambridge University. UK*.

[23]. Meherwan P. Boyce. (2012). Gas turbine engineering handbook. *Gulf Publishing Company. USA*.

[24]. W.W. Bathie. (1984). Fundamentals of Gas Turbines. *Iowa State University of Science and Technology: Ames, IA, USA*.

[25]. G.F.C. Rogers, H.I.H. Saravanamuttoo, Y.R. Mayhew. (1996). Gas Turbine Theory, 4th ed. *Longman Group Limited: London, UK*.